Retrieved Thermodynamic Structure of Hurricane Rita (2005) from Airborne Multi-Doppler Radar Data

Annette M. Boehm and Michael M. Bell

JAS (2021)

Speaker : Mao-Cheng Li

Dec. 13 2022

Outline

- Introduction
- Data and methods
- Kinematic and thermodynamic structure of Hurricane Rita
- Azimuthal-wavenumber analysis
- Summary and conclusions

1. Introduction

- Jones (1995) investigated the impacts of VWS on barotropic vortices and found that the vortex initially tilts downshear, then precesses and eventually reaches an equilibrium tilt direction in the left-of-shear semicircle.

- The effects of diabatic heating were not included in that study as the vortex was dry and barotropic. The potential temperature and vertical velocity anomalies were found to be phase-shifted by 90°, with adiabatic ascent right of tilt, negative potential temperature anomalies downtilt, adiabatic descent left of tilt, and positive potential temperature anomalies in the uptilt direction.

- This pattern is consistent with lifting along isentropes right of tilt, resulting in negative potential temperature anomalies downshear, and adiabatic descent left of tilt, resulting in positive potential temperature anomalies upshear.

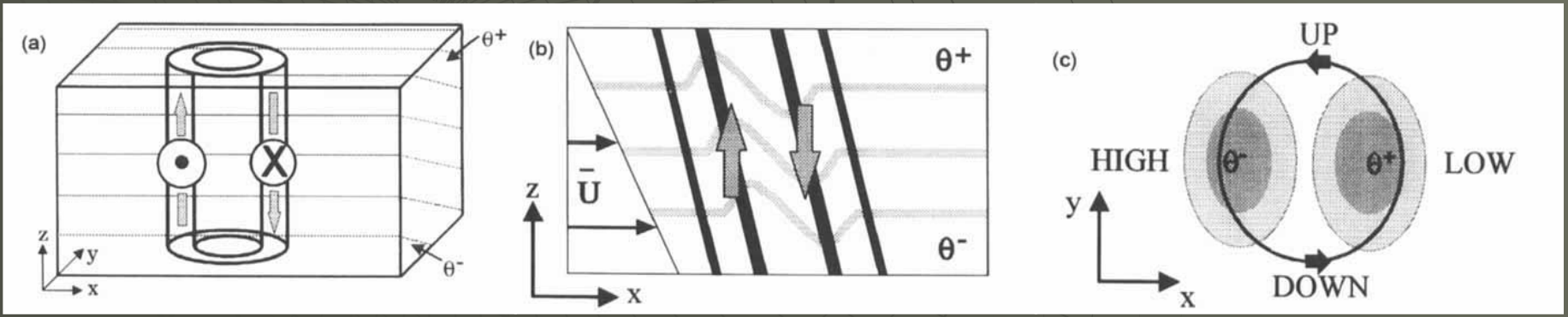

1. Introduction cont.

- The majority of studies addressing the impact of VWS on eyewall convection have focused on the wavenumber-1 structure of wind and precipitation fields. Less attention has been paid to the thermodynamic properties, in part because of a lack of observations.

- Jones (1995) showed that the tilt introduces a thermal couplet. She also mentioned that horizontal advection may act to rotate the thermal anomalies cyclonically with height, whereas vertical advection may act to rotate the thermal anomalies anticyclonically.

- Jones (2000) found an anticyclonic rotation of the temperature anomalies with height and attributed it to the coincident anticyclonic rotation of the tilt with height, keeping the relative orientation of tilt and temperature anomalies constant. She also showed that the temperature anomalies resulted in enhanced low-level stability uptilt, and reduced low-level stability downtilt.

- Axisymmetric conceptual and numerical models of the eyewall are characterized by moist neutral ascent forced by boundary layer convergence. The eyewall is pictured as a ring of mesoscale ascent, with air parcels rising along constant angular momentum surfaces at the speed they obtain leaving the boundary layer (Emanuel 1995).

1. Introduction cont.

- Three-dimensional models suggest that a significant fraction of eyewall convective elements may contain positive buoyancy, with a large fraction of the upward mass transport being accomplished by a few buoyant undilute updrafts (Braun et al. 2006). Observational datasets are necessary to investigate the respective dynamic and thermodynamic contributions to convective forcing in the eyewall.

- Zhang et al. (2000) found that the eyewall is negatively buoyant and the updrafts are driven mainly by the vertical perturbation pressure gradient force, Braun (2002) and Eastin et al. (2005a) found areas of positive buoyancy in the eyewall.

- Axisymmetric TCs are usually considered to be in approximate hydrostatic balance, and in approximate gradient wind balance outside the boundary layer. The gradient balance condition indicates that the bulk of the pressure gradient field is in balance with the primary wind field and does not act to accelerate air parcels radially. The hydrostatic assumption is valid if vertical accelerations are negligible, which is the case for convectively neutral updrafts. This hydrostatic assumption might not be valid for individual updrafts, but it is valid on average for the primary vortex.

- In this framework positive buoyancy translates into upward acceleration unless the vertical perturbation pressure gradient counteracts. This upward acceleration strengthens the secondary circulation, which in turn can enhance the primary circulation and thus intensify the TC.

1. Introduction cont.

- Following this prior research, in the current study we seek to address the following science questions using field observations:

1. What are the mesoscale and convective-scale structures of the thermodynamic fields in the eyewall region?
2. How does vertical wind shear impact the thermodynamic structure?
3. Is the eyewall convectively buoyant?

- Foerster and Bell (2017, FB17 hereafter) developed a new thermodynamic retrieval specifically tailored toward TCs, called Spline Analysis at Mesoscale Utilizing Radar and Aircraft Instrumentation-Thermodynamic Retrieval (SAMURAI-TR).

2. Data and methods — Hurricane Rita

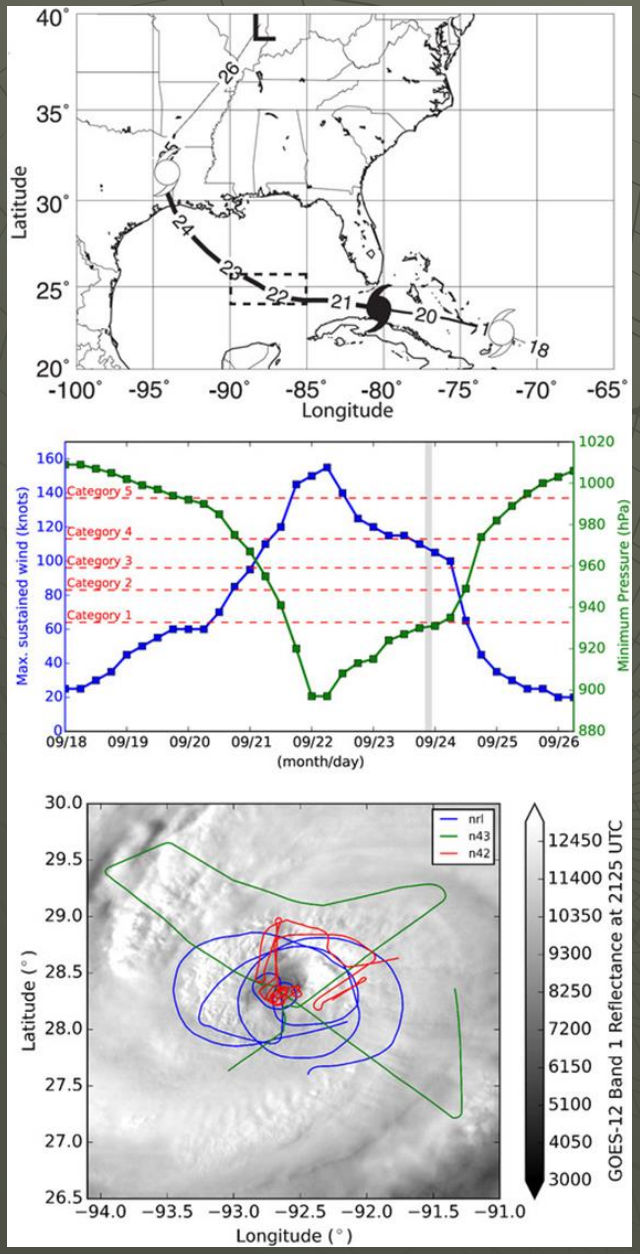

- (top) National Hurricane Center best track position of Hurricane Rita, with the open hurricane symbol denoting tropical storm strength, the closed symbol denoting hurricane strength, and "L" denoting a remnant low.
- (middle) Best track intensity in terms of maximum sustained winds (knots, blue line) and minimum pressure (hPa, green line). The observation period is indicated by the vertical gray bar.
- (bottom) Flight tracks of NRL P-3 (blue), NOAA 43 (green), and NOAA 42 (red) into Hurricane Rita during the period of interest (2020 to 2230 UTC), overlaid on GOES-12 band 1 reflectance at 2125 UTC 23 Sep 2005.

2. Data and methods — Observations

- Divided the analysis into four consecutive periods of approximately 30 min each. Each 30 min period contains enough data to provide a complete view of the entire eyewall, and corresponds roughly to one complete circumnavigation of the eyewall by the NRL P-3.

- The first period lasts from 2022 to 2100 UTC, the second period from 2100 to 2130 UTC, the third period from 2130 to 2200 UTC, and the last period from 2200 to 2235 UTC. The different periods will be referred to by their respective reference times (2040, 2110, 2140, and 2210 UTC), where the storm's center position at reference time is used to define the center position of the respective analysis domain.

2. Data and methods — Retrieval

- The first step is to combine the radar data and complementary in situ flight track, dropsonde and satellite atmospheric-motion-vector observations into a gridded SAMURAI mesoscale analysis.

- The second step of the retrieval method is to calculate the temperature and pressure fields, $\bar{T}(r, z)$ and $\bar{p}(r, z)$, that balance the azimuthally averaged radar-derived wind field using the thermal wind equation. These values of $\bar{T}(r, z)$ and $\bar{p}(r, z)$ are then used as input for the pressure and temperature retrieval SAMURAI-TR.

- The third and final step of the method is the retrieval of the thermodynamic perturbations from the balanced reference state with SAMURAI-TR as described in FB17.

$$\frac{1}{c_p\bar{\theta}_\rho}\left(\frac{\partial u}{\partial t}+u\frac{\partial u}{\partial x}+v\frac{\partial u}{\partial y}+w\frac{\partial u}{\partial z}-fv\right)+\frac{\partial\bar{\pi}}{\partial x}=A=-\frac{\partial\pi'}{\partial x},$$

$$\frac{1}{c_p\bar{\theta}_\rho}\left(\frac{\partial v}{\partial t}+u\frac{\partial v}{\partial x}+v\frac{\partial v}{\partial y}+w\frac{\partial v}{\partial z}+fu\right)+\frac{\partial\bar{\pi}}{\partial y}=B=-\frac{\partial\pi'}{\partial y},$$

$$\frac{1}{c_p\bar{\theta}_\rho}\left(\frac{\partial w}{\partial t}+u\frac{\partial w}{\partial x}+v\frac{\partial w}{\partial y}+w\frac{\partial w}{\partial z}\right)=C=-\frac{\partial\pi'}{\partial z}+\frac{g}{c_p\bar{\theta}_\rho^2}\theta'_\rho,$$

$$\frac{-c_p\bar{\theta}_\rho^2}{g}\left(\frac{\partial A}{\partial z}-\frac{\partial C}{\partial x}\right)=D=\frac{\partial\theta'_\rho}{\partial x}-2\frac{\theta'_\rho}{\bar{\theta}_\rho}\frac{\partial\bar{\theta}_\rho}{\partial x},$$

$$\frac{-c_p\bar{\theta}_\rho^2}{g}\left(\frac{\partial B}{\partial z}-\frac{\partial C}{\partial y}\right)=E=\frac{\partial\theta'_\rho}{\partial y}-2\frac{\theta'_\rho}{\bar{\theta}_\rho}\frac{\partial\bar{\theta}_\rho}{\partial y},$$

- The method solves for the perturbations of density potential temperature θ'_ρ and nondimensional pressure π' using a 3D variational cost function.

3. Kinematic and thermodynamic structure of Hurricane Rita

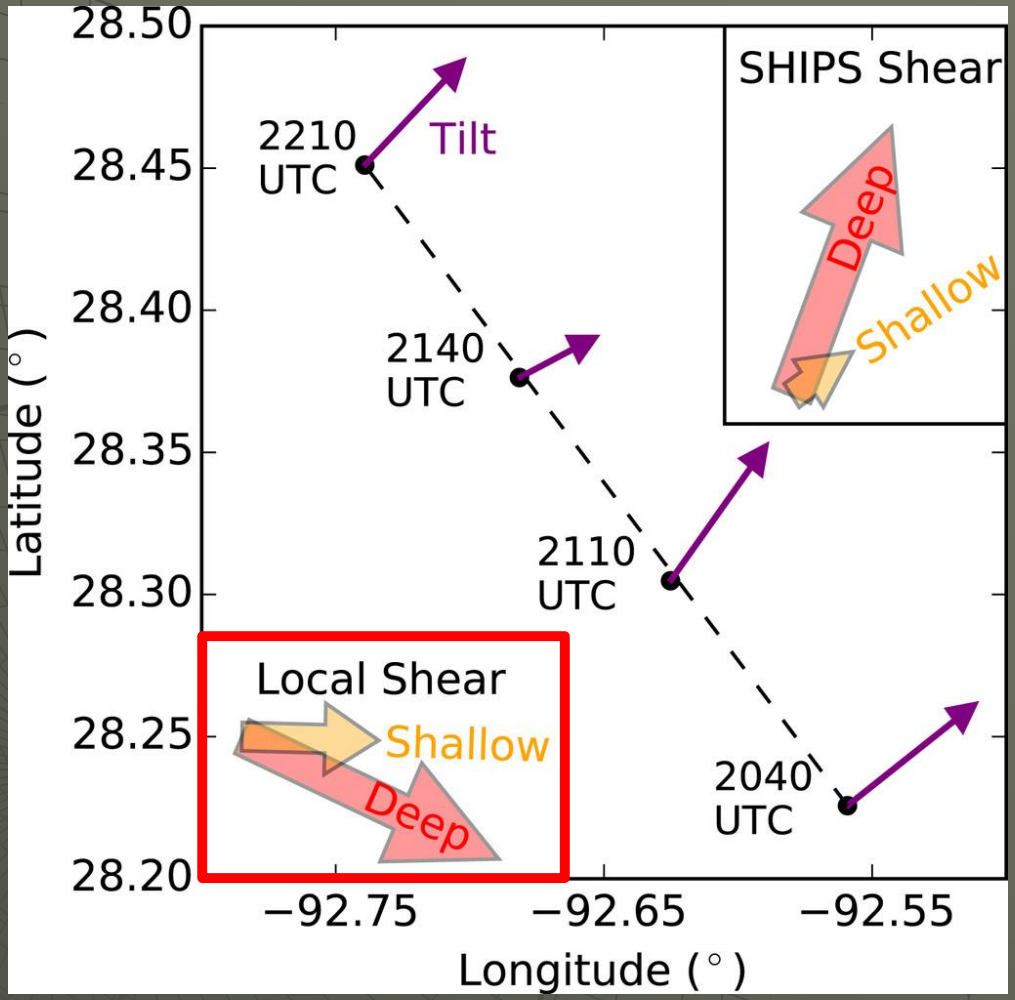

- large-scale Statistical Hurricane Intensity Prediction Scheme (SHIPS) shear (DeMaria and Kaplan 1994)

3. Kinematic and thermodynamic structure of Hurricane Rita cont.

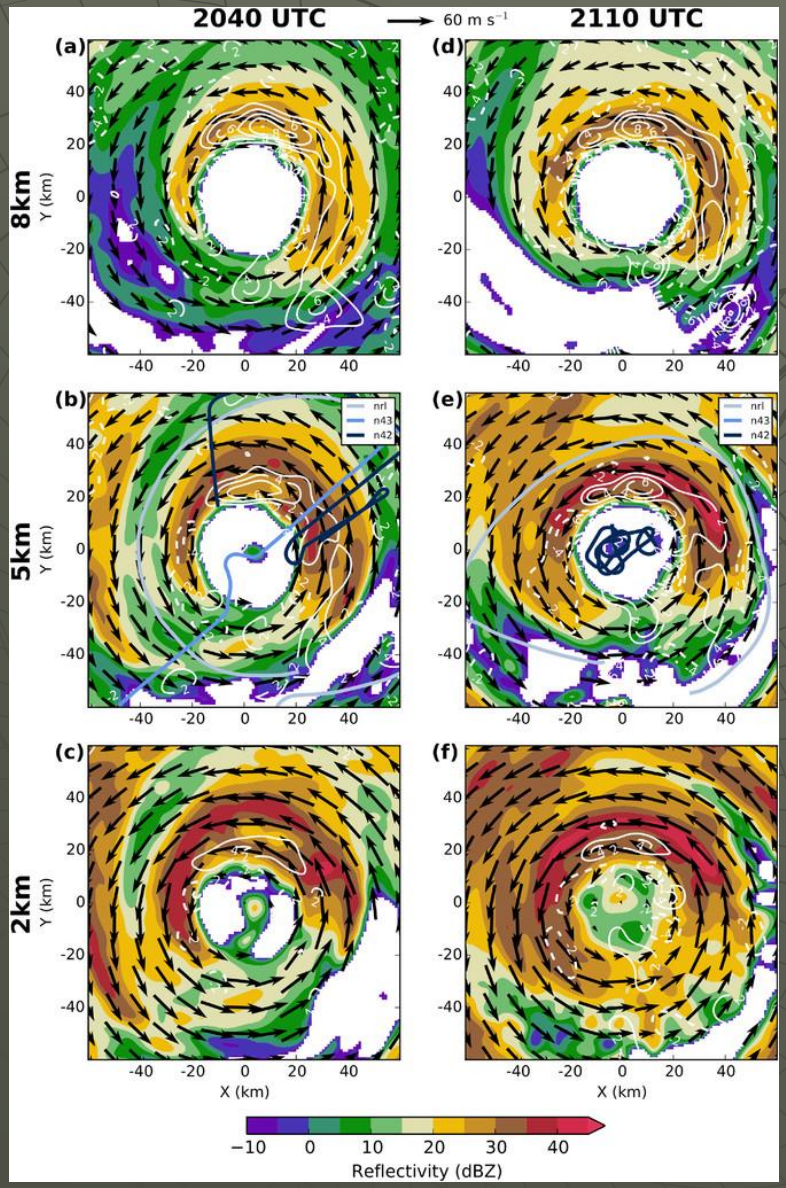

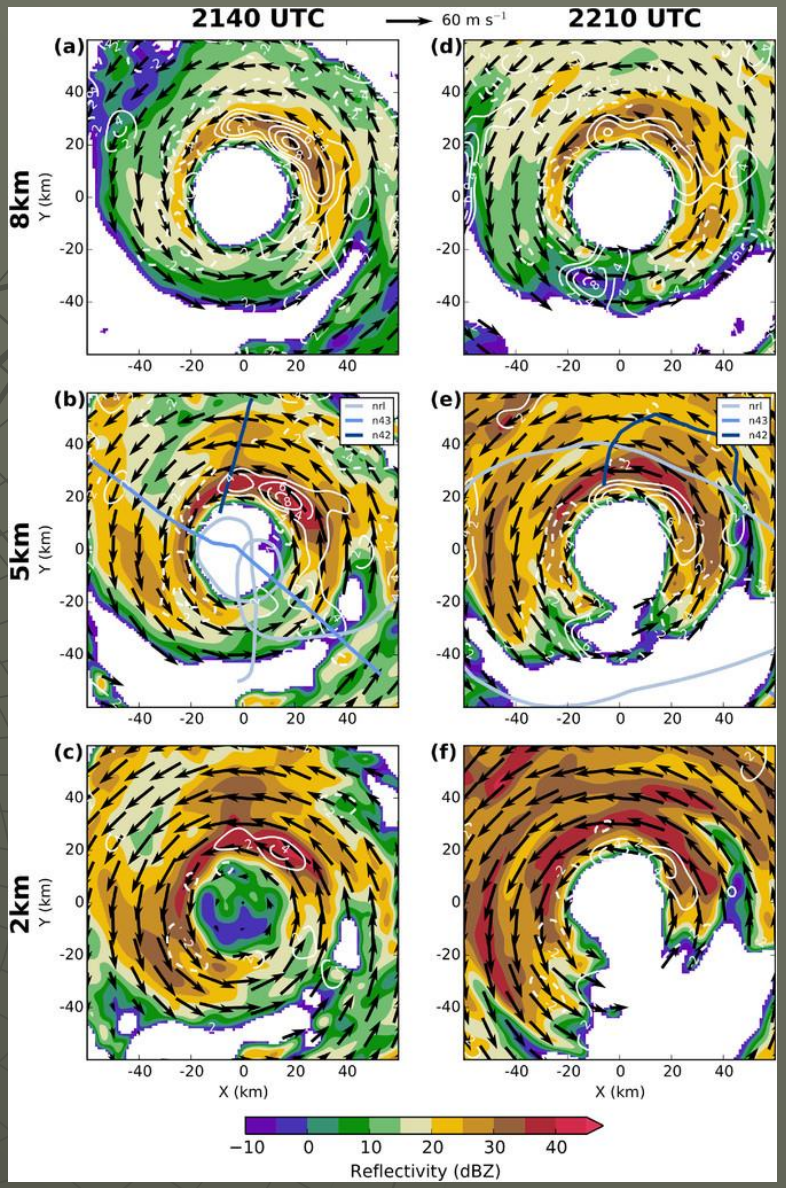

3. Kinematic and thermodynamic structure of Hurricane Rita cont.

Time (UTC)	Center lat (°)	Center lon (°)	Tilt magnitude (km)	Tilt direction (°)
2040	−92.56	28.23	5.0	53
2110	−92.63	28.30	5.0	37
2140	−92.68	28.38	2.2	63
2210	−92.74	28.45	4.2	45

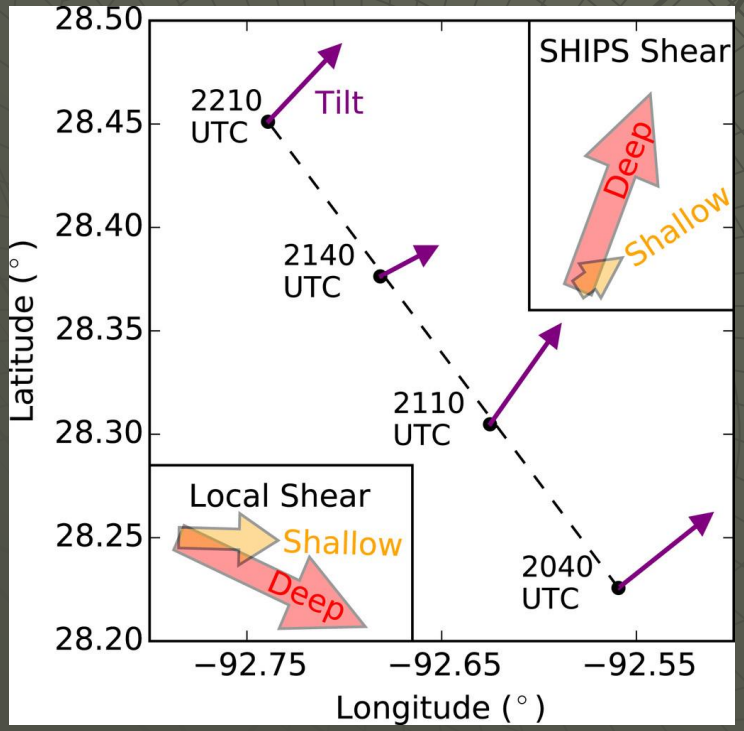

- Rita moved at a speed of 5.3 m s^-1, with a heading of 321°. The vortex tilted to the northeast during all four periods, with the tilt magnitude changing slightly from period to period. The tilt was defined as the difference between the center positions at 8 and 2 km altitudes.

3. Kinematic and thermodynamic structure of Hurricane Rita cont.

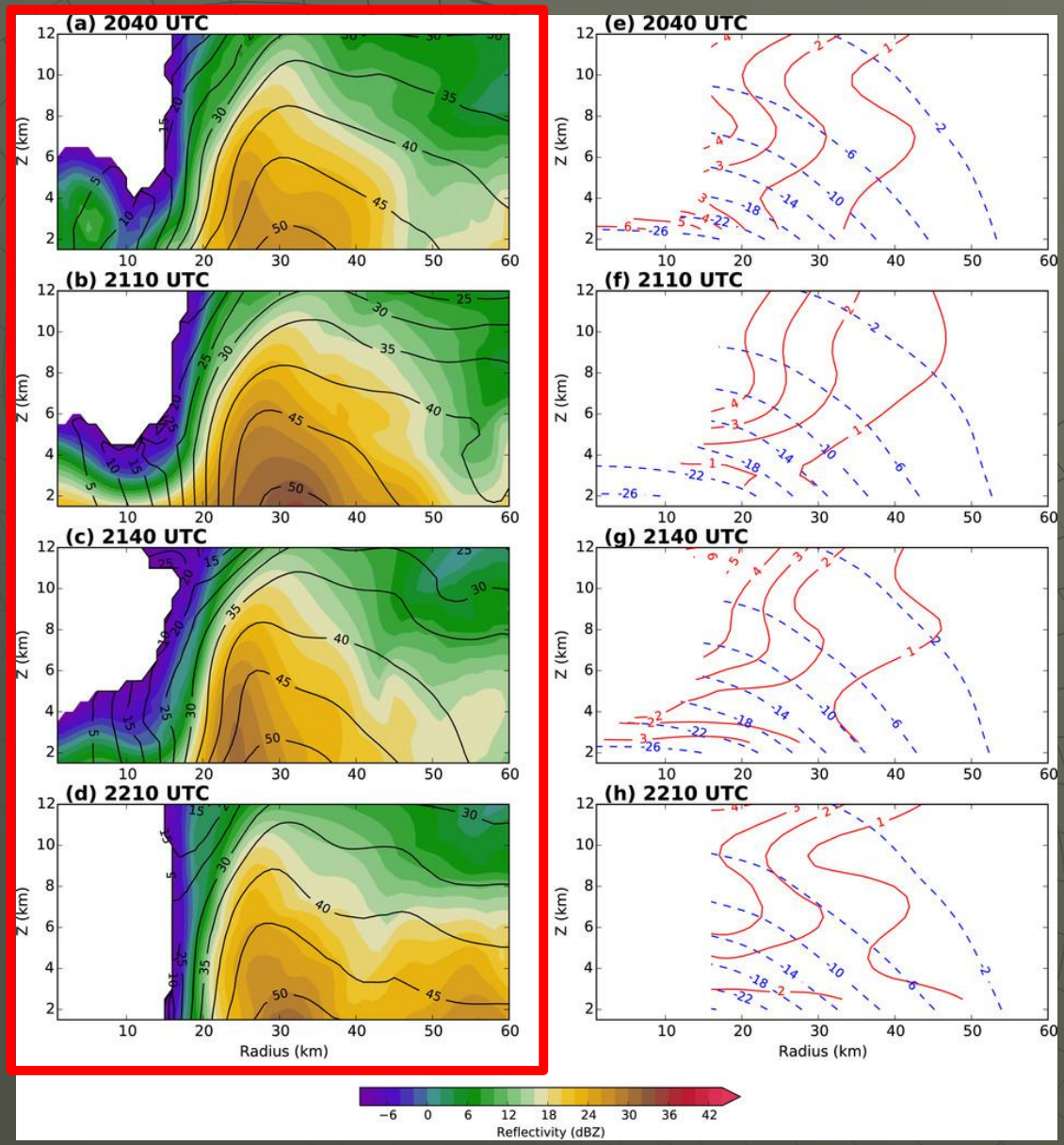

- Maximum azimuthal mean tangential wind speeds in excess of 50 m s^-1 at low levels at a radius of about 30 km during all four periods, and tangential wind speeds exceeding 30 m s^-1 throughout the depth of the domain outside the RMW.
- The radial location of largest mean radar reflectivities ranges from about 25 km (2140 UTC) to about 32 km (2110 UTC); 2210 UTC exhibits an additional radar reflectivity maximum at large radii (around 55 km). At 2110 and at 2210 UTC, the largest mean radar reflectivities are collocated with the largest tangential wind speeds.

3. Kinematic and thermodynamic structure of Hurricane Rita cont.

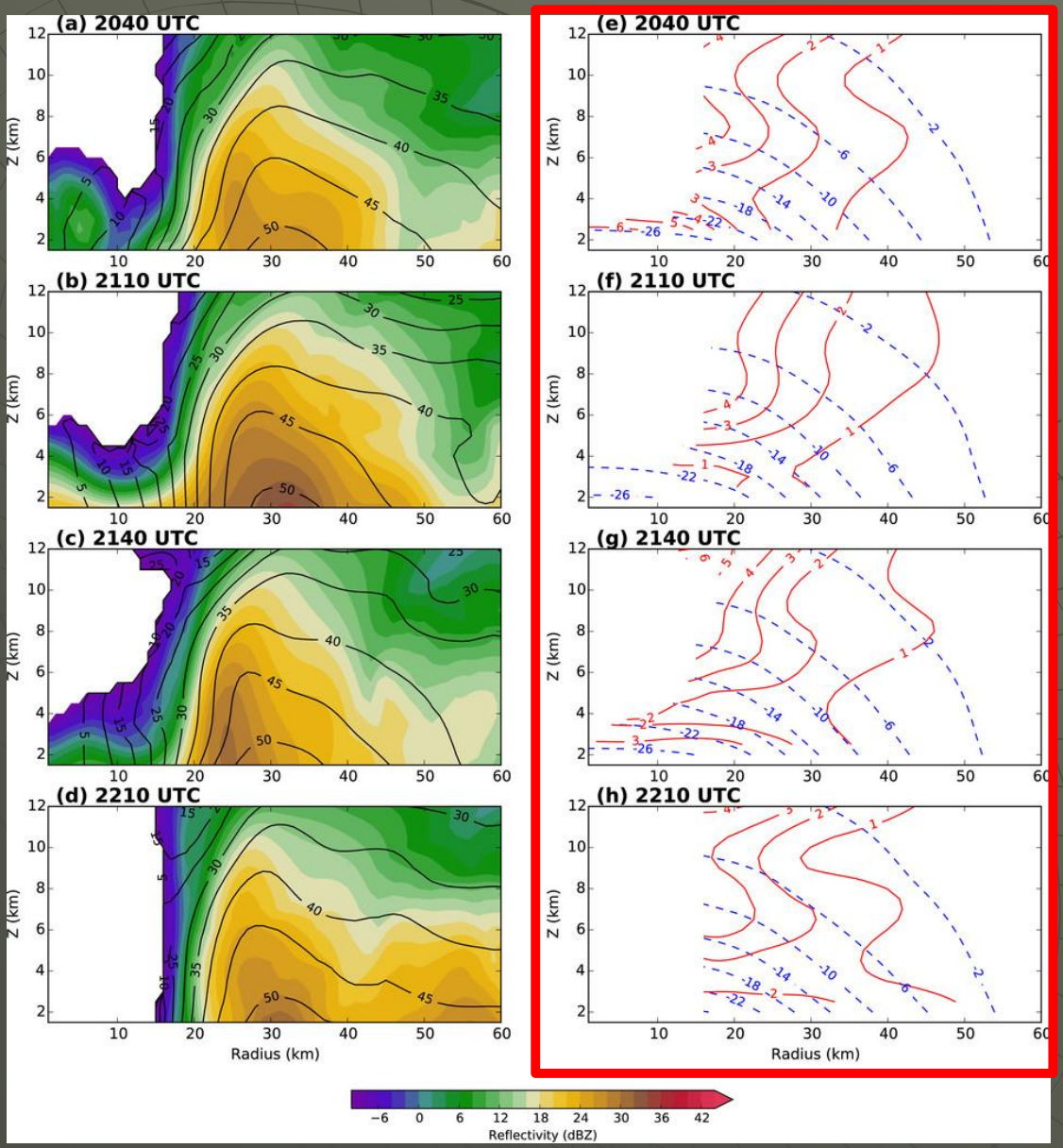

$$[\overline{T}(r, z) - \overline{T}(r = 60\,\mathrm{km}, z)]$$

$$[\overline{p}(r, z) - \overline{p}(r = 60\,\mathrm{km}, z)]$$

- from the edge of the domain toward the center of the storm
- The pressure drop is most pronounced at lower levels, with a maximum pressure drop of $\Delta p >$ 26 hPa in all cases. The temperature increases toward the center, with a minimum at 4 km altitude and maximum from 6 to 9 km altitude.

3. Kinematic and thermodynamic structure of Hurricane Rita cont.

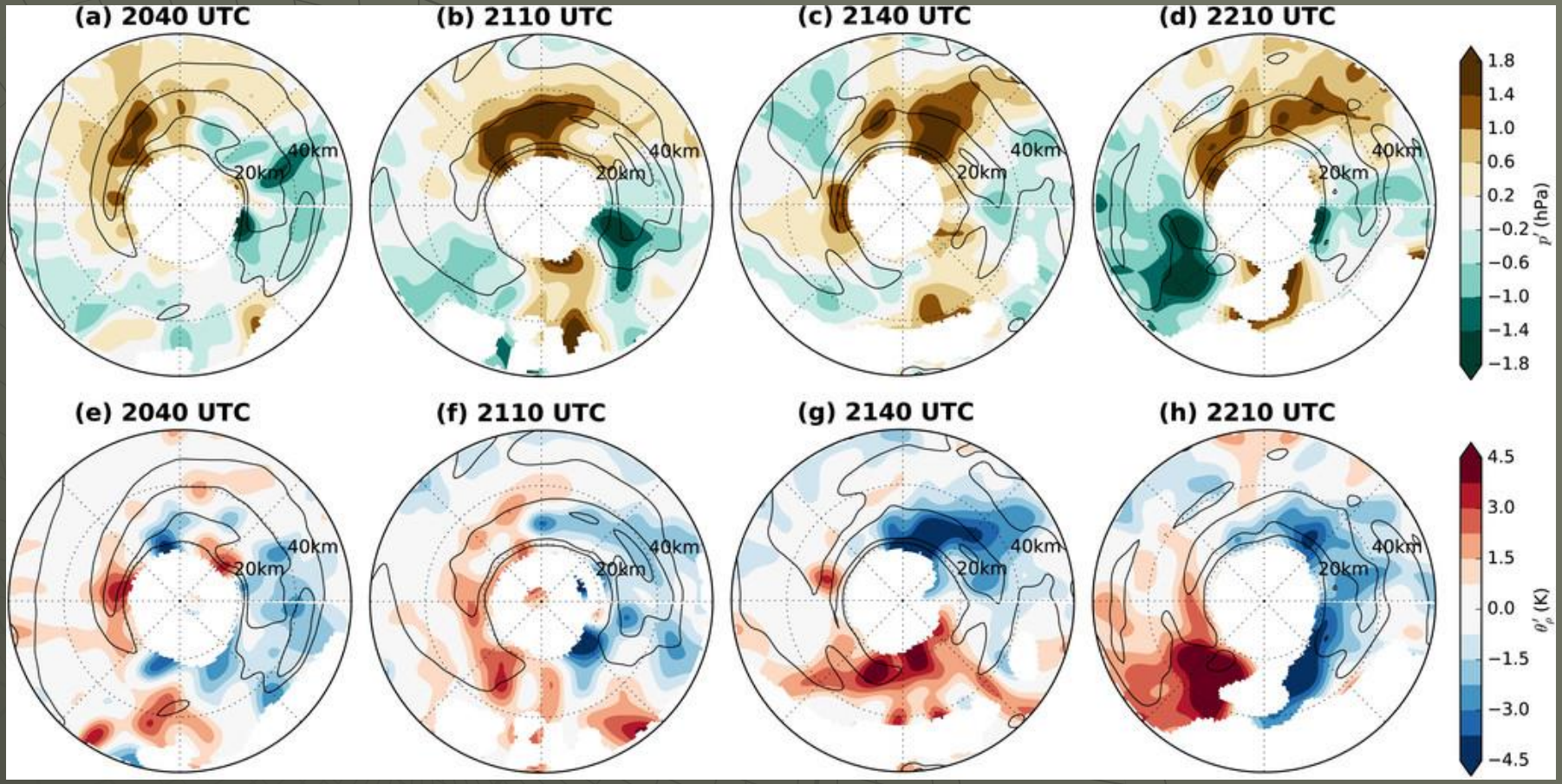

- The retrieved thermodynamic structures show evidence of a wavenumber-1 pattern with additional higher-order structure during all four periods (exemplified here by data at 5 km altitude).

3. Kinematic and thermodynamic structure of Hurricane Rita cont.

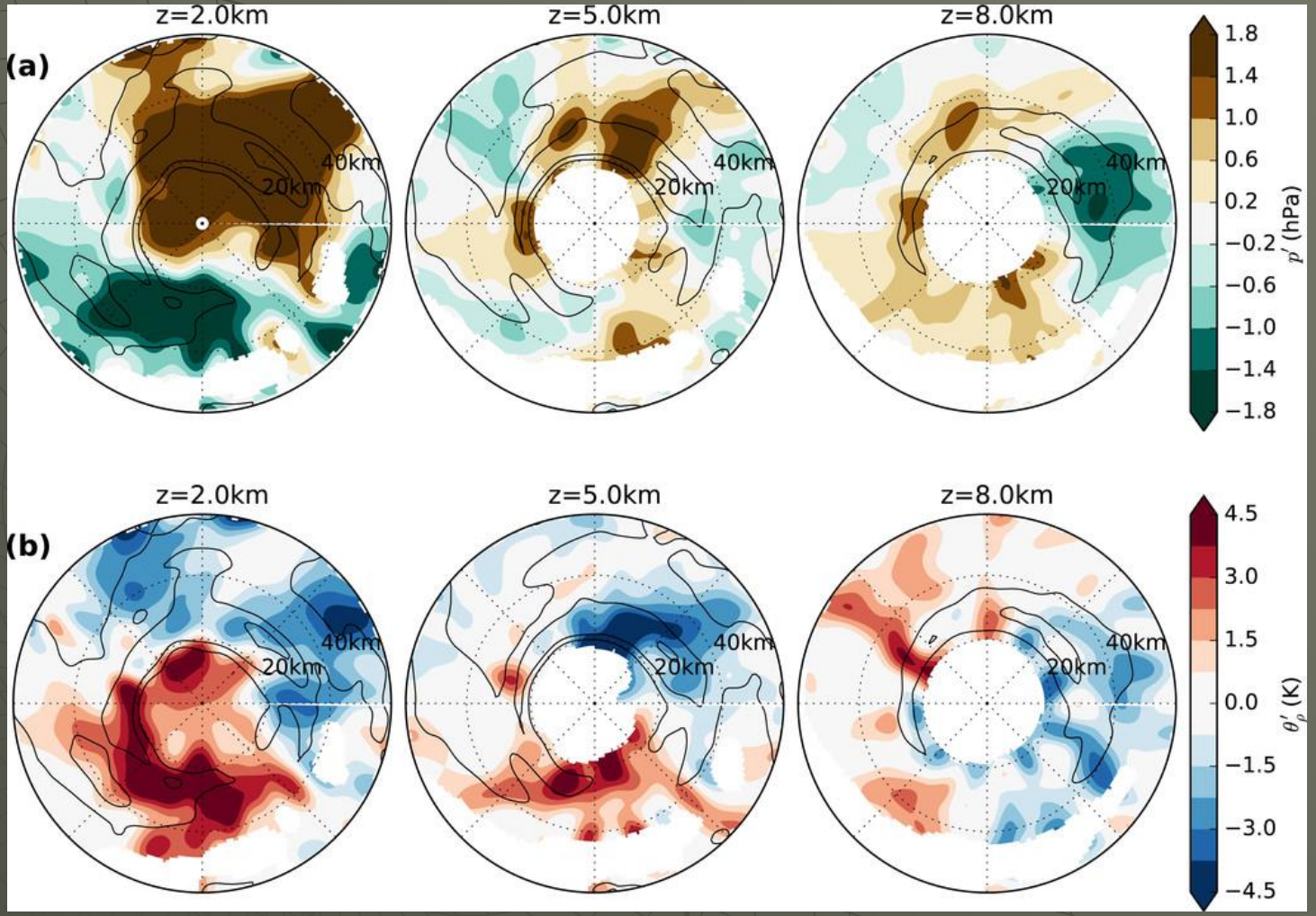

- Horizontal cross sections at different vertical levels (exemplified here by data at three different vertical levels at 2140 UTC) show an azimuthal rotation of the patterns with height.

4. Azimuthal-wavenumber analysis—— Wavenumber-1 structure: Shear

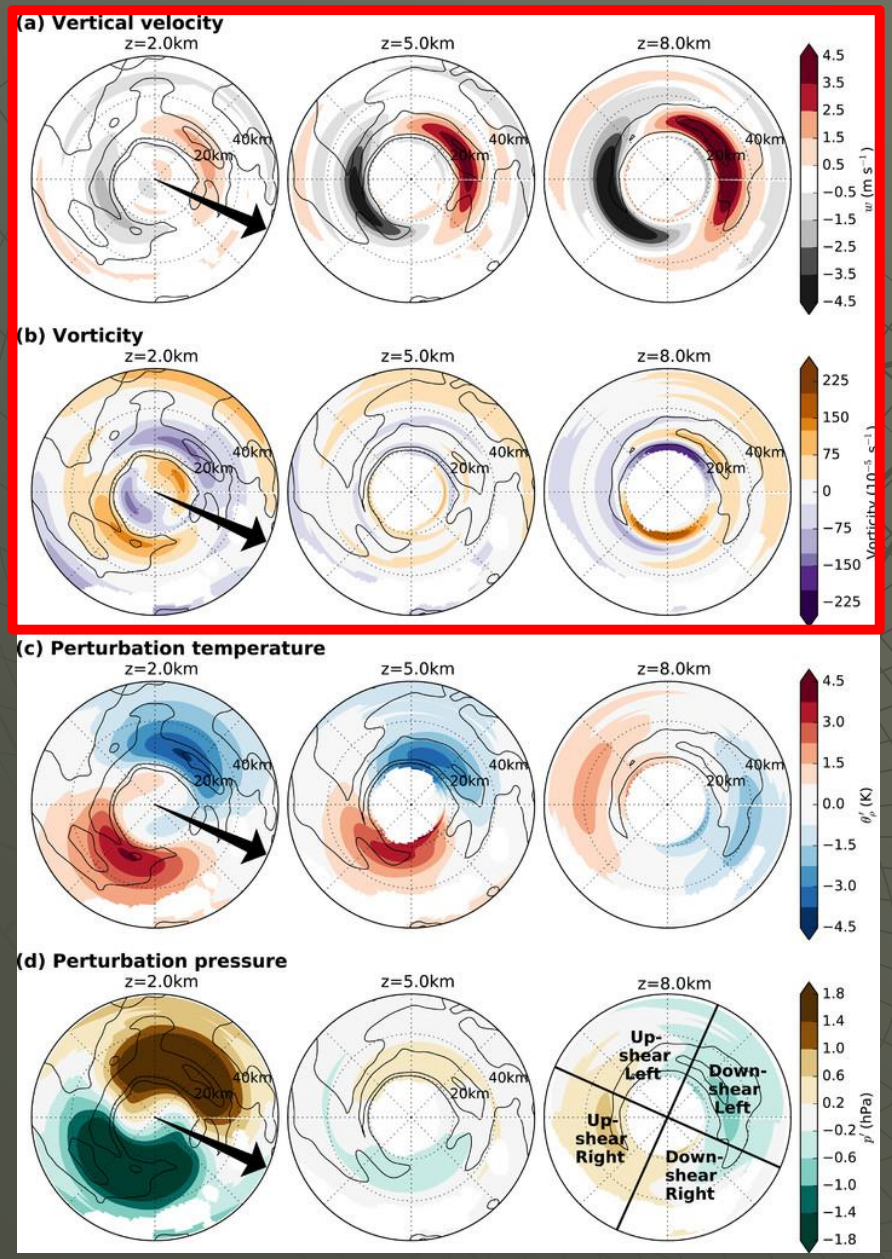

only results for 2140 UTC

- The wavenumber-1 vertical velocity maximum is located in the northeastern eyewall between 20 and 35 km radius for all vertical levels, and the magnitude increases with height. No significant rotation of the vertical velocity with height is evident.
- The wavenumber-1 vorticity asymmetries at 2 km, with one dipole inside the RMW, and an oppositely oriented dipole outside. At 8 km, the convectively active region toward the northeast of the center is collocated with a region of positive vertical vorticity. This pattern might be attributed to vortex stretching in active convection.

4. Azimuthal-wavenumber analysis—— Wavenumber-1 structure: Shear cont.

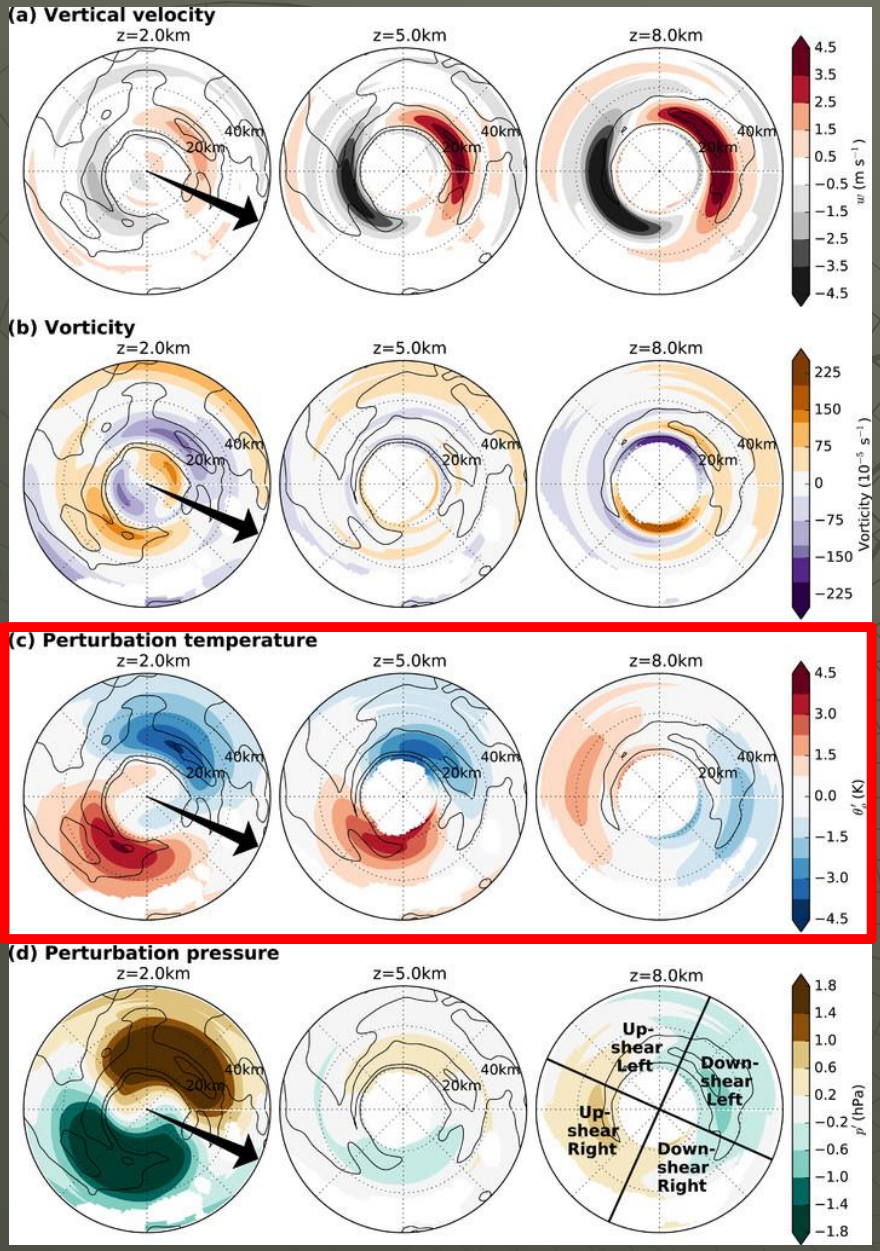

only results for 2140 UTC

- The wavenumber-1 asymmetries of density potential temperature perturbations θ′ρ show a consistent picture over time. The anomalies are maximized around a radius of approximately 30 km, with the azimuthal orientation of the dipole similar for all radii.
- The cold anomalies at 2 km altitude are located in the northeastern part of the eyewall, and at 8 km they are located in the eastern part of the eyewall, resulting in an anticyclonic rotation with height. The magnitude of the temperature anomalies decreases with height.

4. Azimuthal-wavenumber analysis—— Wavenumber-1 structure: Shear cont.

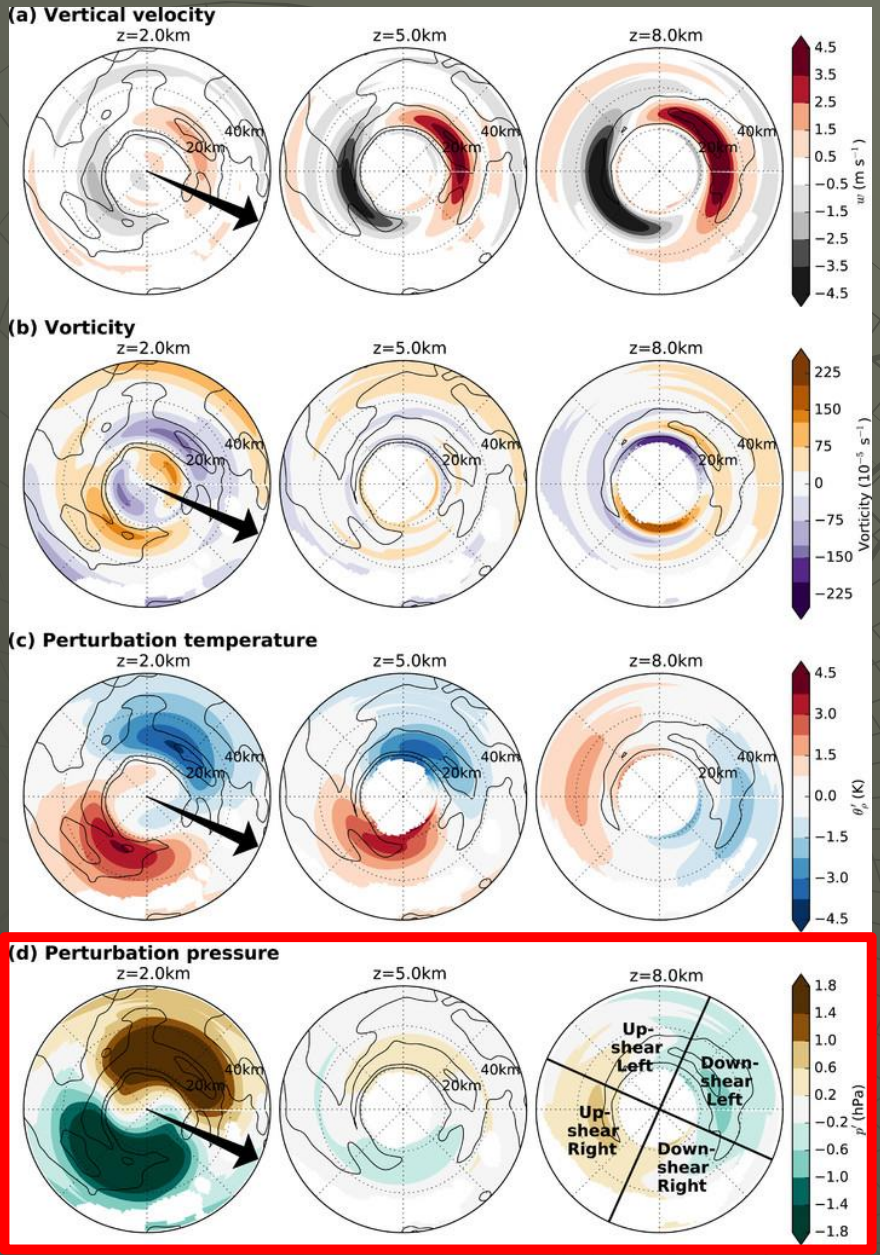

only results for 2140 UTC

- The wavenumber-1 asymmetries of perturbation pressure p′ also show a consistent picture over time. The pressure perturbations are maximized around a radius of approximately 30 km similar to the temperature perturbations.
- In contrast to the temperature perturbations, however, the pressure perturbations rotate cyclonically with height. At 2 km, the positive pressure perturbations are located in the northeastern part of the eyewall. At 8 km, the positive pressure perturbations are located in the western part of the eyewall. The pressure perturbations are weakest at midlevels.

4. Azimuthal-wavenumber analysis—— Wavenumber-1 structure: Shear cont.

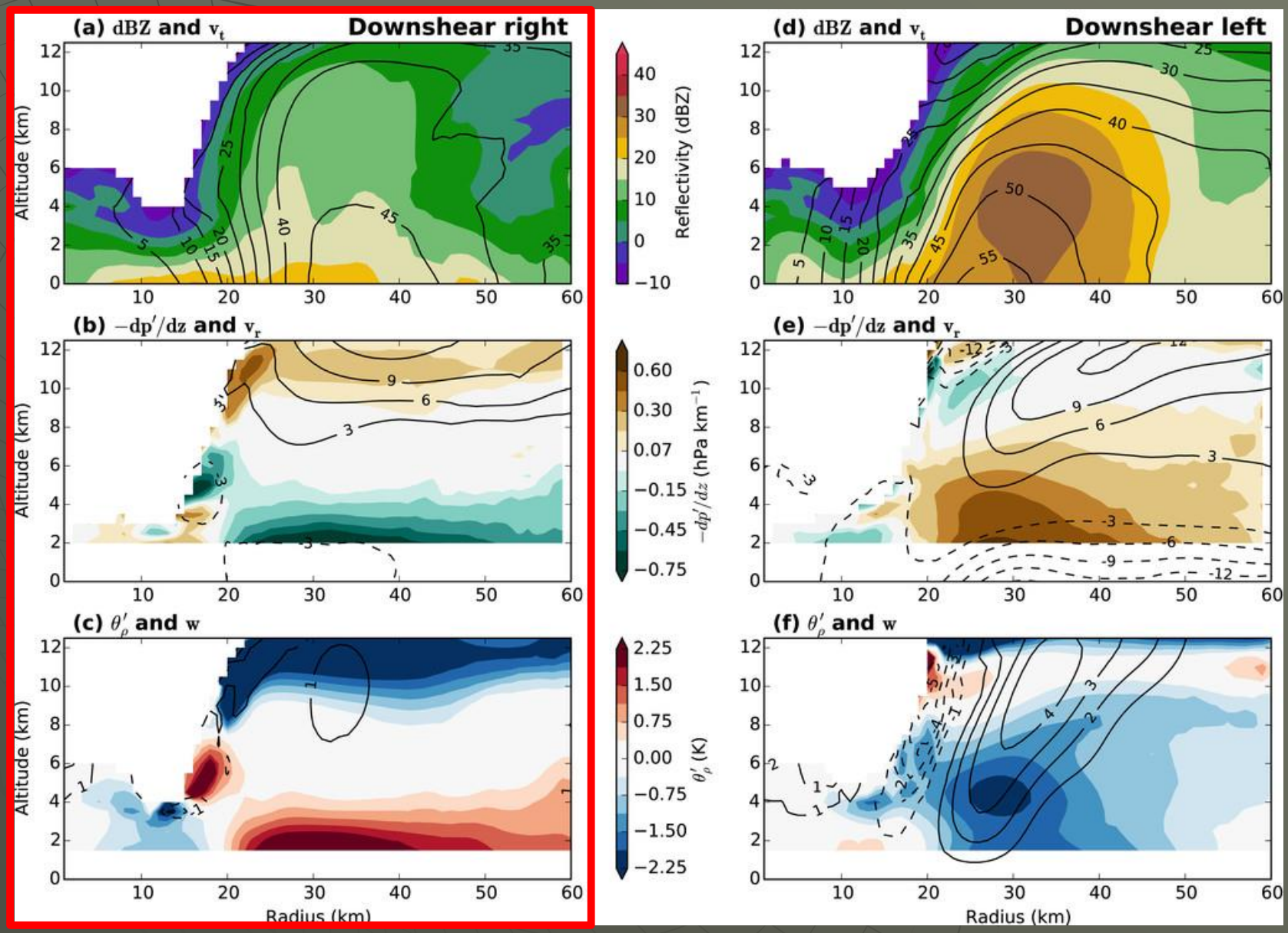

4. Azimuthal-wavenumber analysis—— Wavenumber-1 structure: Shear cont.

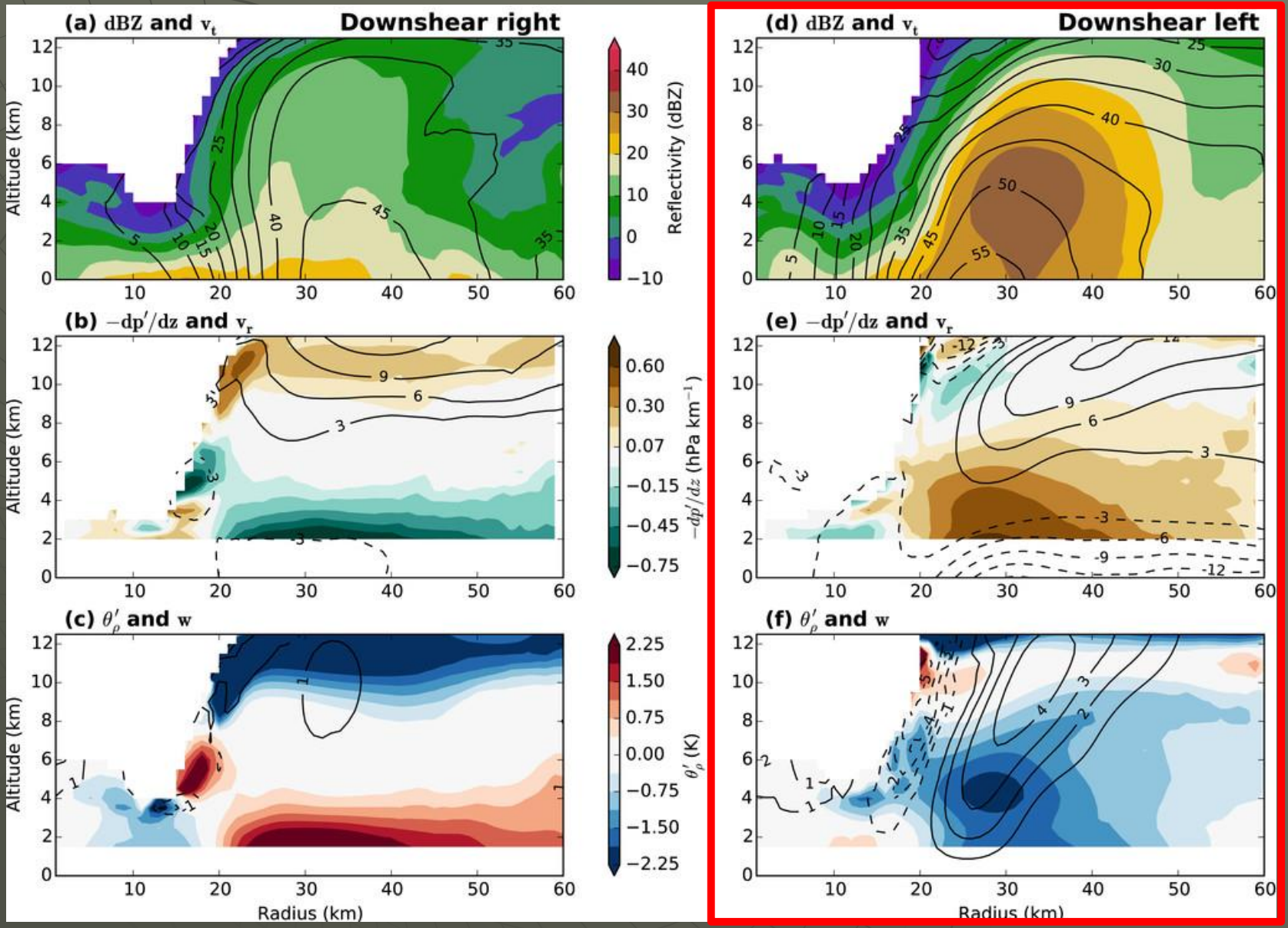

4. Azimuthal-wavenumber analysis—— Wavenumber-1 structure: Shear cont.

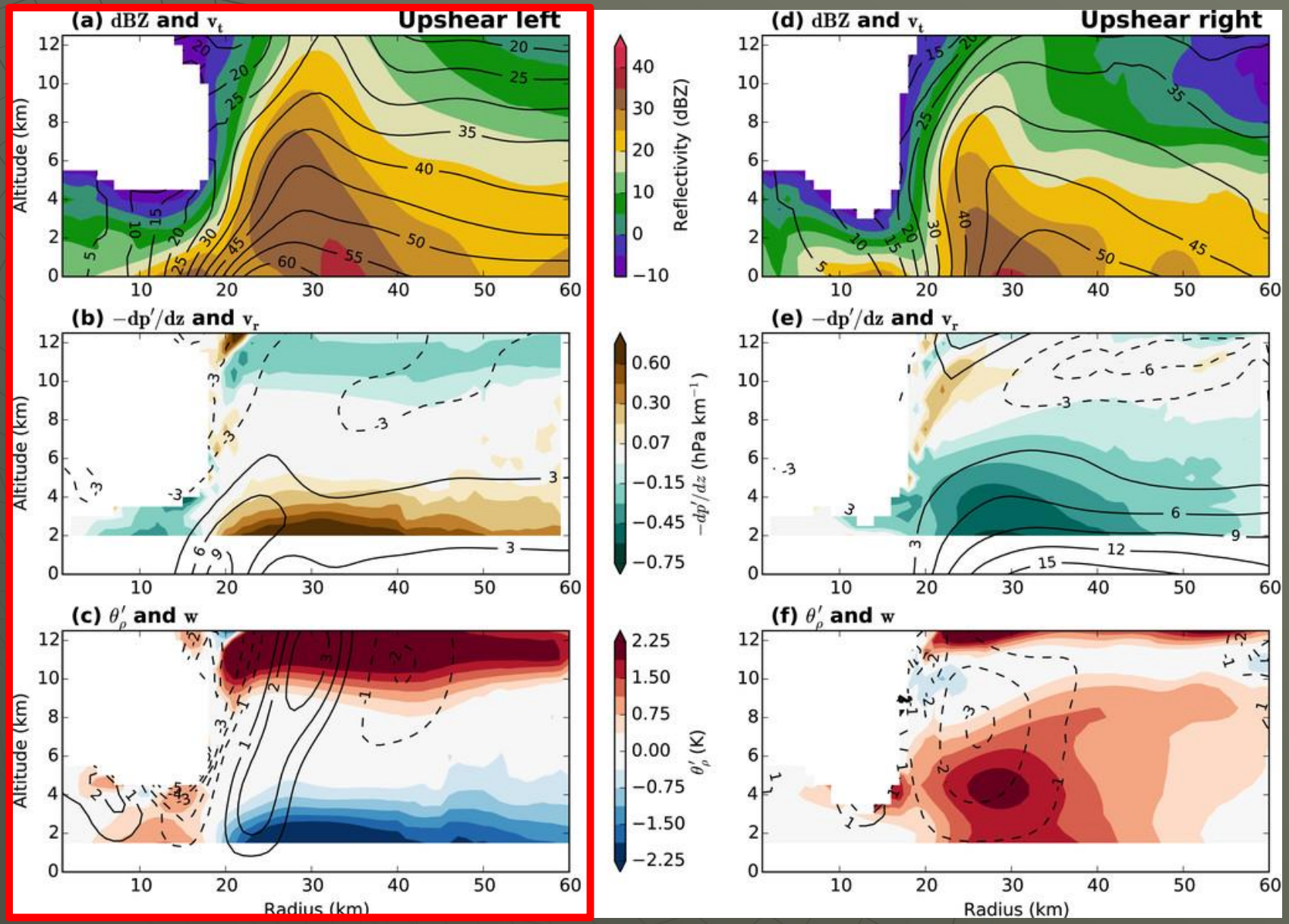

4. Azimuthal-wavenumber analysis—— Wavenumber-1 structure: Shear cont.

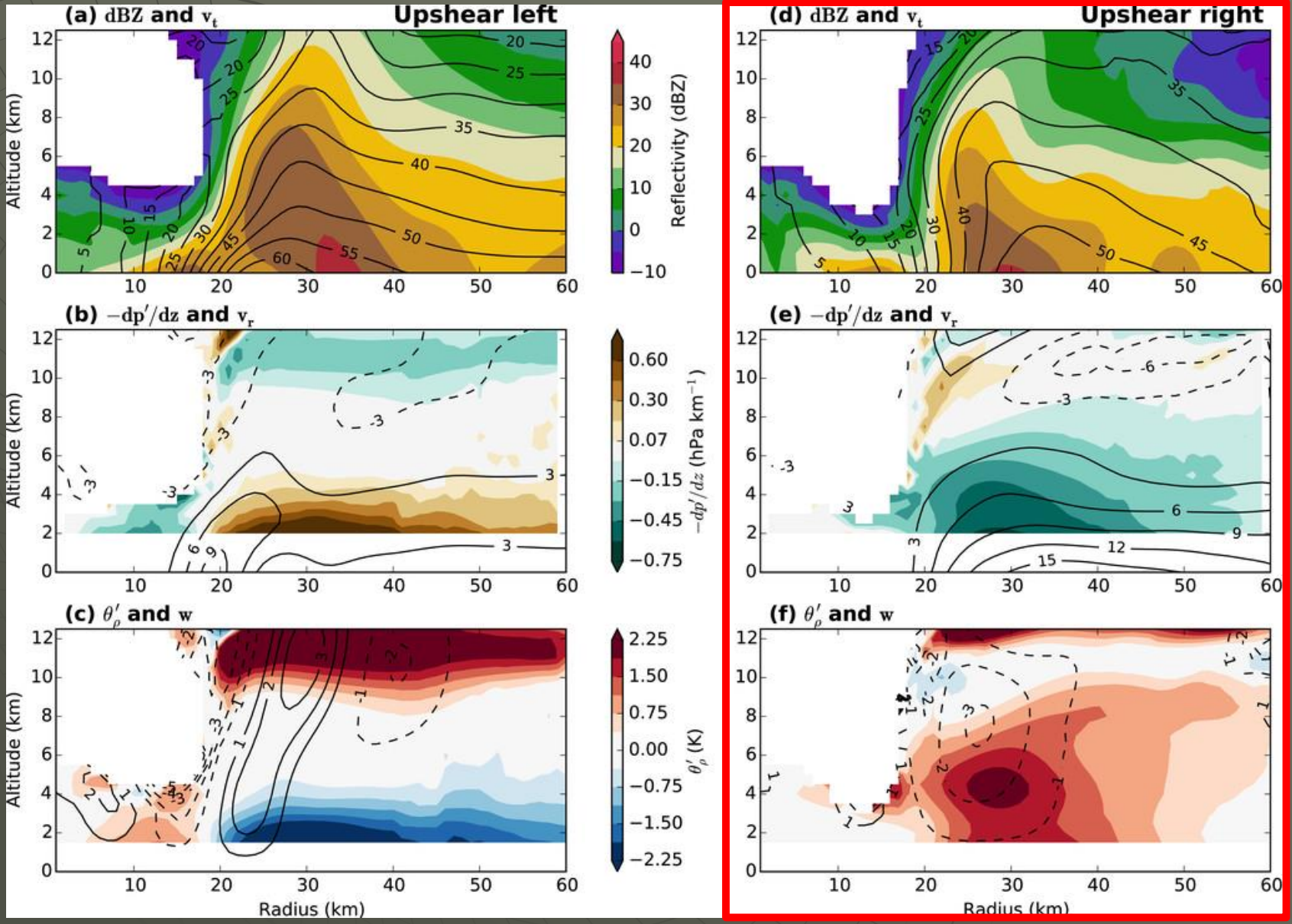

4. Azimuthal-wavenumber analysis—— Wavenumber-1 structure: Shear cont.

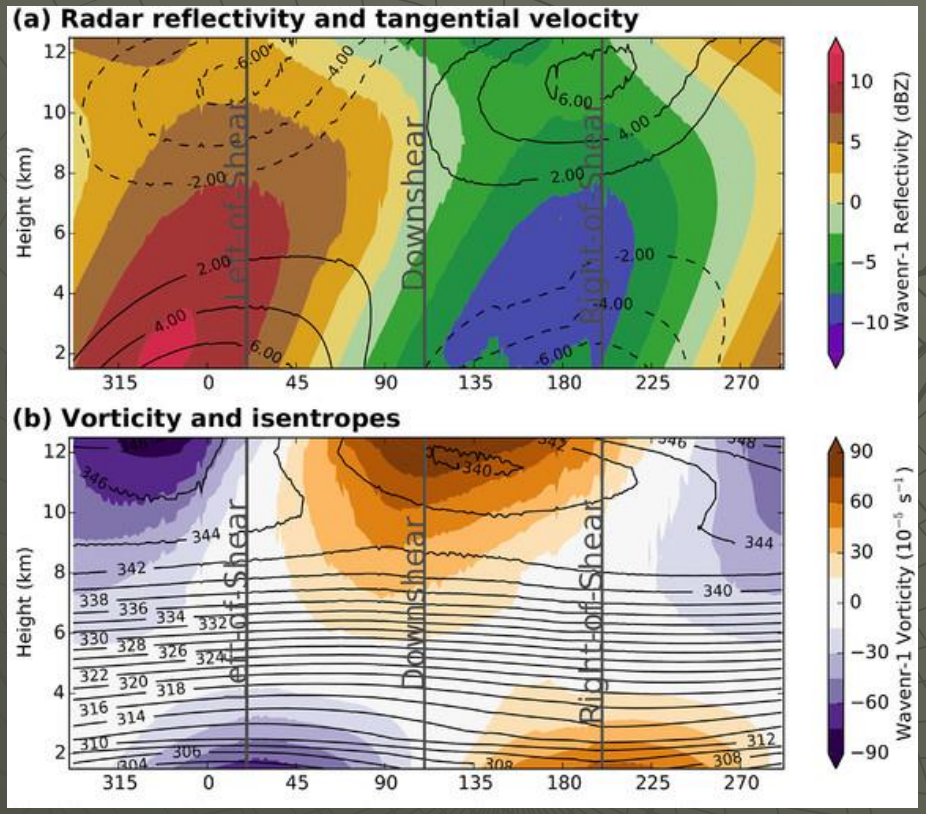

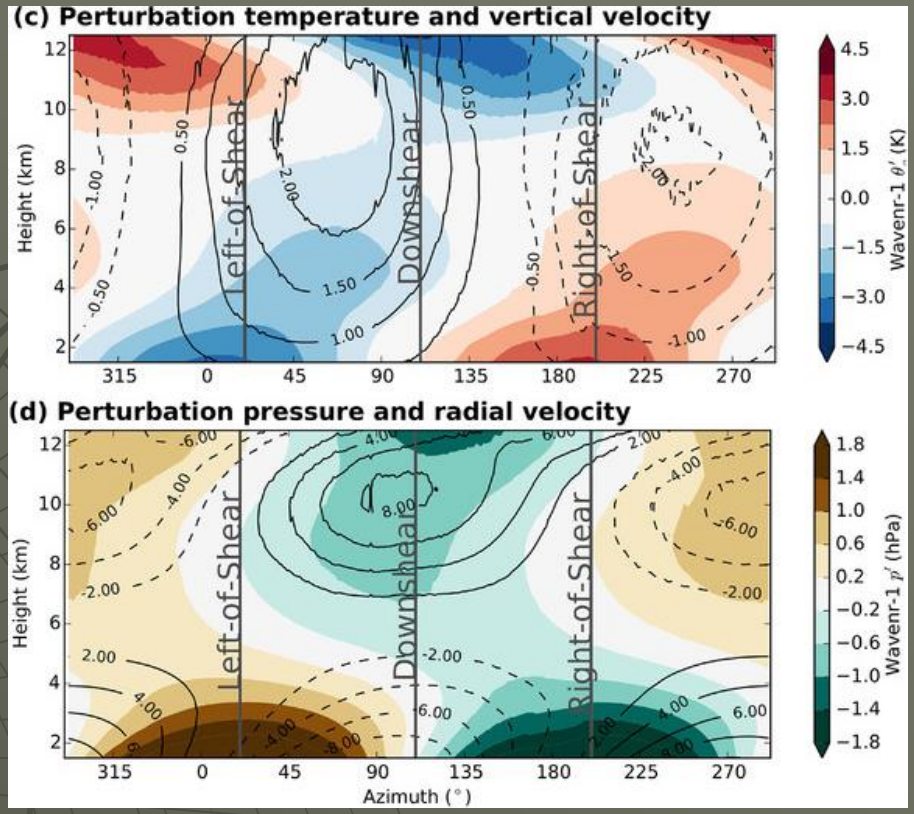

- upshear left downshear-left downshear right upshear-right

4. Azimuthal-wavenumber analysis—— Higher-order wavenumbers: Eyewall convection

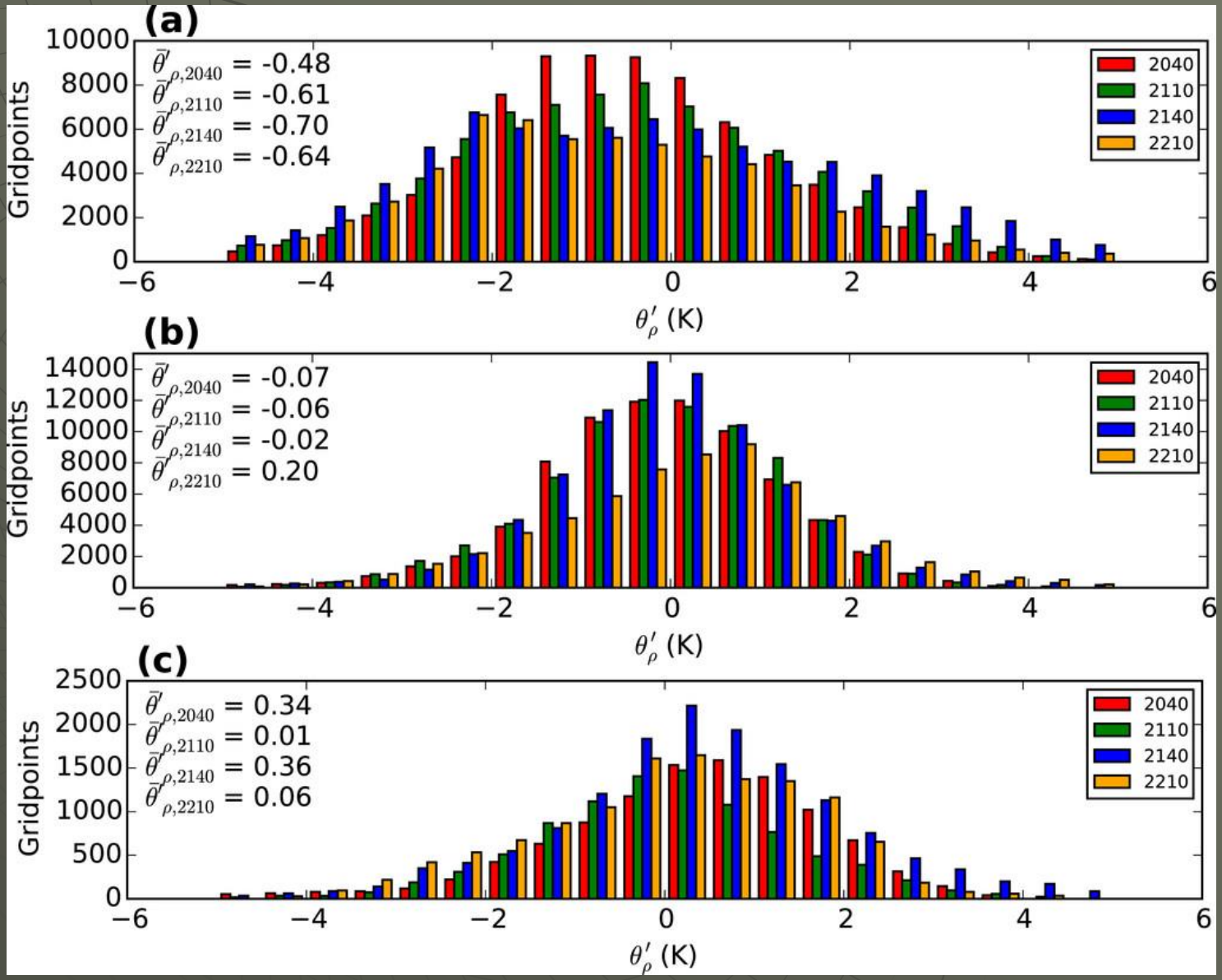

4. Azimuthal-wavenumber analysis—— Higher-order wavenumbers: Eyewall convection cont.

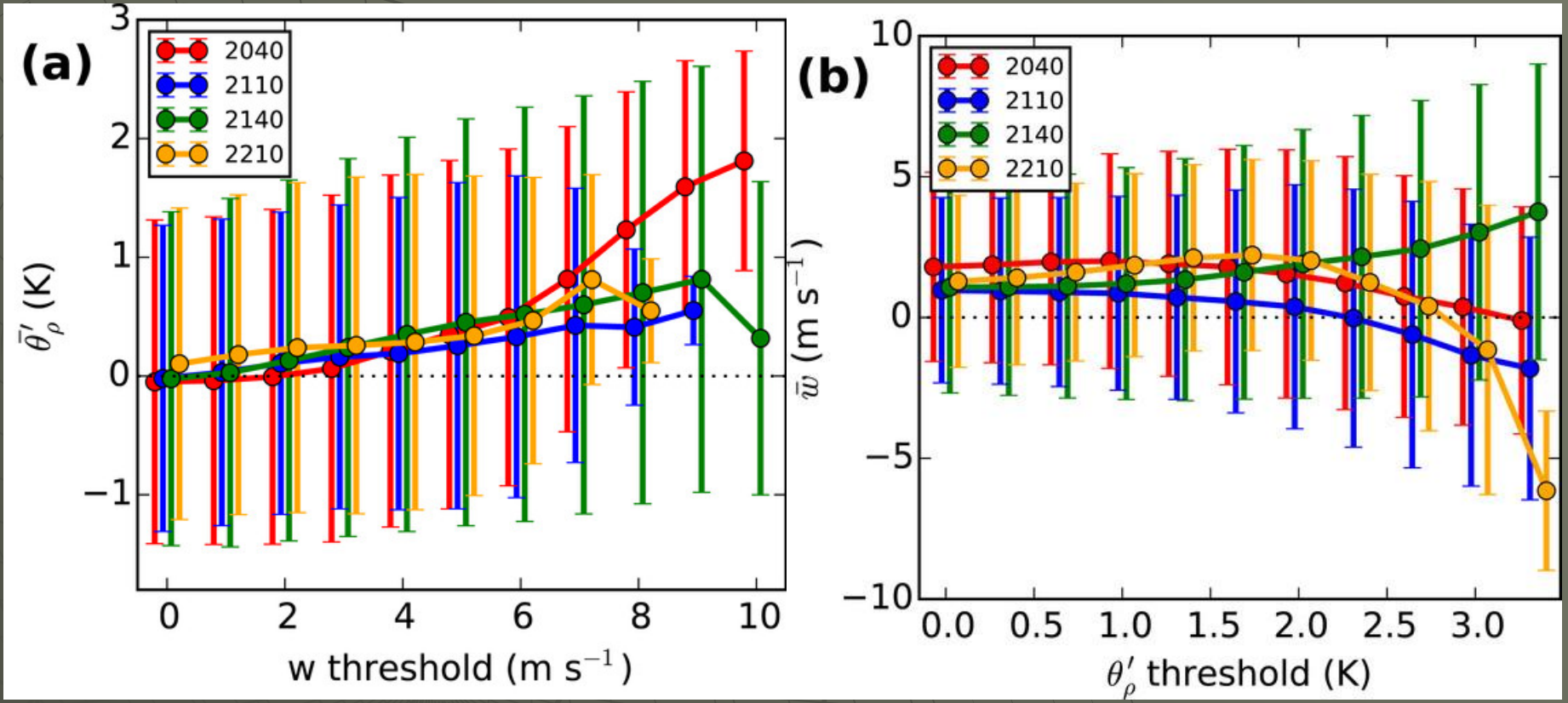

- To test the robustness of this result, average temperature perturbations for grid points exceeding a certain vertical velocity threshold are computed. Thresholds are chosen as increments of 1 m s^−1, from 0 to 10 m s^−1.

4. Azimuthal-wavenumber analysis—— Higher-order wavenumbers: Eyewall convection cont.

$$\frac{1}{c_p \overline{\theta}_\rho} \frac{Dw}{Dt} = -\frac{\partial \pi'}{\partial z} + \frac{g}{c_p \overline{\theta}_\rho^2} \theta'_\rho$$

	2040 UTC	2110 UTC	2140 UTC	2210 UTC	Total
Wnrs 0&1, dynamic	0.02	0.00	0.00	0.01	0.00
Wnrs 0&1, thermodynamic	0.00	0.00	0.00	0.01	0.00
Wnr $\geq$ 2, dynamic	0.15	0.19	0.03	0.26	0.14
Wnr $\geq$ 2, thermodynamic	0.39	0.58	0.28	0.47	0.42

4. Azimuthal-wavenumber analysis—— Higher-order wavenumbers: Eyewall convection cont.

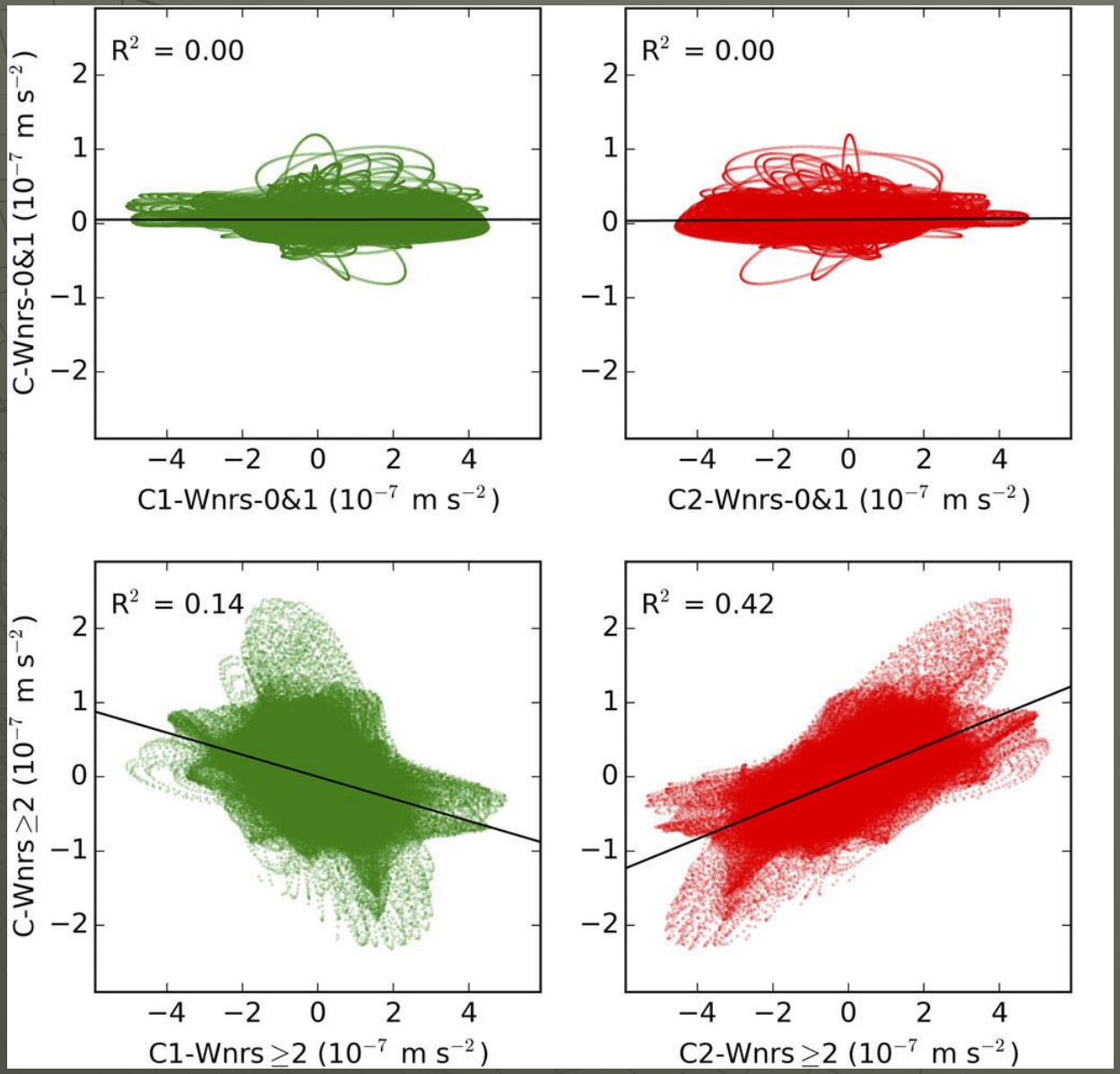

5. Summary and conclusions

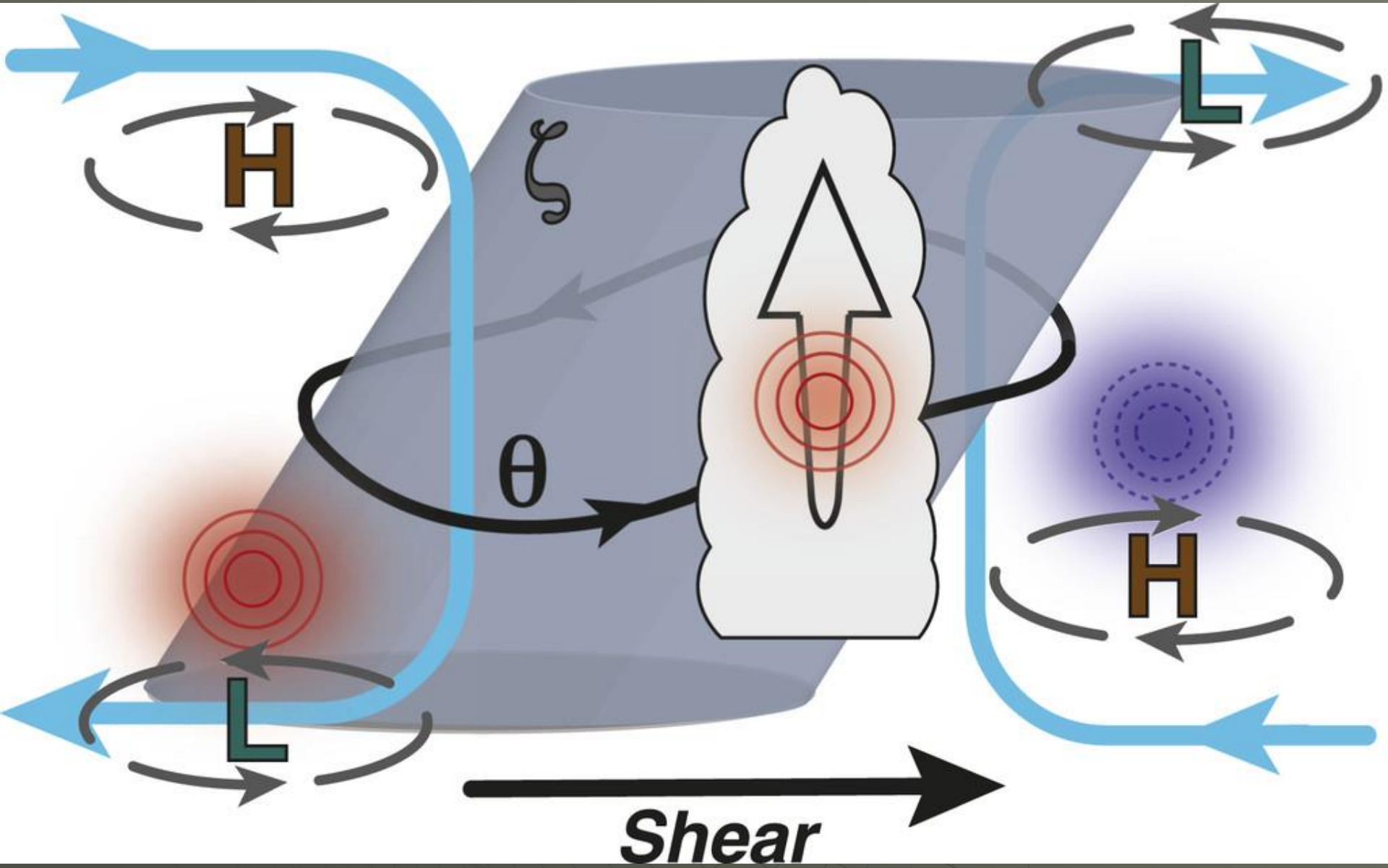


The End…
Thanks !
Questions??